



The effect of low concentrations of polypyrrole on the structural, thermal, and dielectric characteristics of CMC/PPy blends

Amira M. Salem¹, A. Raouf Mohamed¹, and A. Y. Yassin^{2,*}

¹ Physics Department, Faculty of Science, Port-Said University, Port-Said, Egypt

² Department of Basic Sciences, Delta University for Science and Technology, Gamasa, Mansoura, Egypt

Received: 6 April 2023

Accepted: 4 July 2023

Published online:

14 July 2023

© The Author(s) 2023

ABSTRACT

The current work aims to synthesize carboxymethyl cellulose/polypyrrole (CMC/PPy) blends with different PPy concentrations as promising blends for energy storage devices with low cost and excellent chemical and physical characteristics. The structural and dielectric characteristics of CMC/PPy blends were studied. FT-IR spectroscopy is utilized to study the structural properties of the present blends, whereas the dielectric properties are explored at frequency range of 0.1 Hz–20 MHz. The structural study of CMC/PPy blends showed good homogeneity between the CMC matrix and PPy as a conductive filler. The thermal behavior of the present blends was also investigated using DSC, where the thermal stability of the blends was improved after incorporating PPy into the host matrix. The dielectric characteristics results indicated a rise in the dielectric parameters of CMC with an increase in the PPy content up to 8 wt%. The dielectric parameters of CMC/PPy blends are frequency dependents. The dielectric constant (ϵ') and AC electrical conductivity of the blends under study enhanced by about 33% with a rise in the PPy content to 8 wt%. The dielectric loss (ϵ'') values decreased from 3.4938 to 0.93071 at 10 kHz; this performance means that the CMC/PPy blends have an excellent possibility for energy storage devices with low dielectric loss in various applications, such as sensors, batteries, and capacitors.

1 Introduction

The high demand for thin, malleable, transparent, thermally stable, and electrically conductive films is growing. Such conductive films pave the way for potential applications, including supercapacitors, 3D

printing, solar cells, polymer light-emitting diodes, sensors, flexible touch screens based on these films, and sustainable energy systems [1]. Several researchers are looking into developing novel transparent conducting materials to meet these ever-increasing needs. Many promising materials have been used with

Address correspondence to E-mail: a_yassin2200@yahoo.com; ahmed.yassin@deltauniv.edu.eg

transparent conductors, such as conductive polymers [2, 3], metallic grids [4], and nanofillers [5–8] to form novel materials with the required features. Samples transparency in the visible/infrared spectra and their high electrical conductivity are among the most compelling arguments in favour of producing a transparent and electrically conductive material [1].

The polymer blending method is one of the cheapest and most successful approaches. It is an effective method for developing materials with a wide range of applications and for creating novel polymeric materials with optimal physicochemical characteristics. The final blend should be customized to the application's requirements, which is impossible to do with only one of the polymers used.

CMC polymer is made from cellulose and is therefore safe to use, recyclable, widely available, biocompatible, and environmentally beneficial [9, 10]. Films made with CMC are very transparent and mechanically strong, making them ideal for use in a wide range of commercial applications [11], including but not limited to textiles, varnishes, paints, medications, foods, and cosmetics.

PPy is also a promising polymer with high electrical conductivity, large energy storage ability, and can be easily synthesized. Electronic devices and chemical sensors are the most popular applications based on PPy and other conductive polymers. Although PPy has some excellent properties, including electrical conductivity, it also has some disadvantages, such as low mechanical properties, poor thermal stability in the air, and mechanical instability after doping [12, 13]. The applications of PPy have been limited due to its fragile, brittle, rigid, and non-biodegradable properties.

Dey and Kar [14] reported the photoluminescence emission intensity of PPy/PMMA blends. They found that the increase in the blend's emission relative to pure PPy resulted from Forster resonance energy transfer between the two materials. Uzunçar et al. [15] incorporated CMC into PPy a biocompatible sensor platform, where PPy, utilized as a plasticizer, and enhanced conductivity, whereas CMC improved the hydrophilicity of the final product. Although many studies have been carried out on films composed of CMC and PPy, there has yet to be a direct and satisfactory study of their dielectric and thermal characteristics and the extent to which structural qualities influence these aspects. Therefore, adding CMC will help overcome some of the

drawbacks of PPy because of the existence of a highly concentrated carboxylic group throughout the backbone and the ability to produce good films.

Here, various features of PPy/CMC blends, including structural analysis using FT-IR, were thoroughly investigated. Meanwhile, these samples' conduction mechanism, relaxation performance, and dielectric results have been comprehensively analyzed. These studies comprehensively understand the effect of varying PPy concentrations on CMC's structural and electrical characteristics. Moreover, they will profit by deploying the finished product in various applications, such as sensors, batteries, and capacitors with the best features.

2 Experimental method

2.1 Materials

The CMC polymer with a MW of 25×10^4 was acquired from BDH Chemical Ltd. in Poole, United Kingdom. On the other hand, PPy was bought from Sigma Aldrich. As the universal solvent, distilled water was used throughout the film processing.

2.2 Blends preparation

CMC powder (3.5 g) is dissolved in double-distilled water (350 mL) by stirring until a suitably viscous solution is created. The PPy solution was then slowly diluted with 50 mL of DW while being continuously agitated after dissolving CMC and PPy in double-distilled water and constantly stirring under the same circumstances. The CMC solution was then filled with different quantities of PPy (0, 4, 8, 10, and 12 wt%), which were denoted by pure CMC, CMCPy-1, CMCPy-2, CMCPy-3, and CMCPy-4, respectively.

To eliminate any trace of solvent and form a pure CMC film for comparison, the viscous solution was poured onto clean glass Petri plates and dried in an oven at 50 °C for two days. We removed the films from the Petri dishes after they were dry and put them in vacuum desiccators for later use. Pieces of blended films with the correct dimensions were cut.

2.3 Analysis techniques

Fourier transform infrared analysis (FT-IR) absorption spectra was obtained at room temperature for

various films made of CMC filled with different concentrations (0, 4, 8, 10, 12) of PPy using a single beam FT-IR spectrometer (FT-IR-430, JASCO, Japan). The materials' FT-IR spectrum was obtained in the $4000 - 500 \text{ cm}^{-1}$ spectral range to analyze their structures. Discovery SDT 650 - DSC & TGA all-in-one was used for the thermogravimetric analysis of the prepared samples at different contents of PPy. The samples were heated from room temperature to $500 \text{ }^\circ\text{C}$ with increasing temperature at a heating rate of $10 \text{ }^\circ\text{C}$ per minute in nitrogen atmosphere in platinum cell. The dependence of AC electrical conductivity on temperature 298 K and frequency range 0.1 Hz to 20 MHz was investigated with the use of a programmable automatic (Model Hioki 3531Z Hitester).

3 Results and discussions

3.1 FT-IR analysis

FT-IR spectroscopy plays an effective role in detecting the structural changes and interaction between carboxymethyl cellulose and polypyrrole. Figure 1 depicts the FT-IR absorption spectra of pure CMC, PPy, and CMC/PPy blends at room temperature in the region $4000 - 500 \text{ cm}^{-1}$.

The characteristic bands of CMC observed in Fig. 1 can be assigned as follows; the stretching vibrations of hydroxyl groups ($-\text{OH}$) appeared at around 3200 cm^{-1} . The CH_2 asymmetric stretching vibrations were recorded at about 2923 cm^{-1} [16], whereas the vibrational peak at 1720 cm^{-1} is attributed to the $-\text{CO}$ absorption peak in $-\text{COOH}$ [17]. The vibrational band around 1586 cm^{-1} relates to $\text{C}=\text{O}$ stretching, and the $\text{C}-\text{H}$ scissoring occurs at about 1415 cm^{-1} . The absorption peak at 1262 cm^{-1} was the $\text{C}-\text{C}$ stretching vibration peak [18]. The stretching vibrational $\text{C}-\text{O}^-$ band at 1057 cm^{-1} of pure CMC is observed [19]), and $\text{C}-\text{O}$ stretching of carbonyl groups present on the CMC backbone at 1102 cm^{-1} . The peak appeared at 1456 cm^{-1} for the CMCPPy-2, CMCPPy-3, and CMCPPy-4 samples, having an intensity of 0.0174, 0.0214, 0.0135 and 0.0212, respectively, because of the presence of $\text{C}-\text{N}/\text{C}=\text{N}$ stretching vibration in PPy [17, 18, 20].

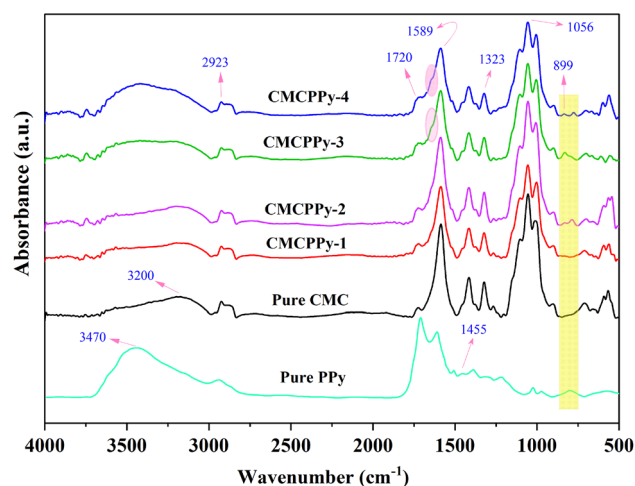


Fig. 1 FT-IR spectra of pure CMC, PPy, and CMC/PPy blends at room temperature in the region $4000 - 500 \text{ cm}^{-1}$

After PPy was added, the band intensity at 1323 cm^{-1} decreased and shifted to lower wavenumber 1321 cm^{-1} ($-\text{OH}$) [19]. It is also noticed a slight increase and shift in the 899 cm^{-1} peak, ascribed to the $\text{C}-\text{H}$ out-of-plane deformation in PPy [18]. Compared with the pure CMC spectrum, the incorporation of PPy with concentrations of (4, 8, 10, and 12 wt%) gave rise to a slight shift in wavenumber with the increase of broadness and decrease in intensity. This change indicates the considerable interaction of coordination inside the CMC/PPy blend at the asymmetrical (COO^-) stretching of the carboxylate anion of ($\text{C}=\text{O}$) and ($\text{C}-\text{O}^-$) [21]. The absorption peak at 3200 cm^{-1} shifted to 3422 cm^{-1} due to the involvement of the hydroxyl groups in the blend formation and the overlapping of the $-\text{OH}$ of CMC and $-\text{NH}$ groups of polypyrrole in the blended network [20].

The new peaks at 3567 cm^{-1} and 3526 cm^{-1} are attributed to the asymmetrical $\text{N}-\text{H}$ stretching from PPy entrapped in the polymer blend, which would enhance the transport features. It could be explained that the re-association of ion and ion aggregation formation resulted in an increase and decrease of conductivity in the existing system depending on the region's intensity of most interactions that happened between the host polymer and dopant at ($2800 - 400$) and ($2000 - 900$). A similar mechanism has been recorded in which it is thought that H^+ originating from $\text{N}-\text{H}$ begins to overcrowd if a certain amount of

dopant is added. When PPy is included in polymer blend systems, the COO⁻ stretching of (C=O) carboxylate anion is the region where most ion contact occurs. FT-IR analysis is utilized in this research to study ion dissociation and association coexistence.

Table 1 summarizes the wavenumber shifts for all CMC/PPy blends doped at the different functional groups. According to the table, When PPy was introduced into the present system, proton H⁺ from PPy reacted with oxygen from CMC via the Grotthuss mechanism [19, 21]. As seen from the above, hydrogen bonding and coordination interaction of H⁺ significantly impact the (COO). These actions occurred via coordinating the host polymer's (CMC) site (oxygen) and so conduction should occur. The blending process is complex and interactive [21].

3.2 Differential scanning calorimetry (DSC)

DSC measures energy flows into and out of a material in response to temperature changes associated to macromolecular transitions induced by heat. DSC curves of pure CMC and CMCPpy-x (x = 1, 2, 3, and 4) blends were analyzed to determine the differences in their thermal behavior and get information about temperatures of different phase transitions. Figure 2 displays a series of endotherms up to 500 °C, the lowest corresponding to the glass transition temperature (T_g). Due to the miscibility of the blend's component polymers, a single T_g is observed.

The pure CMC thermogram shows a relatively broad endothermic glass transition around 73 °C [22]. However, the T_g value of CMC/PPy blends increased

from 80 to 93 °C for CMCPpy-1 and CMCPpy-4, respectively. The change in T_g confirms the effective interfacial interaction through the polar groups of CMC and PPy. The increase in T_g with the addition of PPy indicates the rigidity of the prepared blends [23]. Table 2 exhibits the T_g, T_c, T_m, and T_d values for pure CMC and CMCPpy-x (x = 1, 2, 3, and 4) blends. The broad endothermic dip at 272 °C represents the melting temperature (T_m) of the pure CMC host polymer. The T_m of the blends was increased to 280 and 295 °C for CMCPpy-1 and CMCPpy-2 films, respectively. Further, the shifts in T_g and T_m values, as summarized in Table 2, confirm the effective incorporation of PPy into the CMC segments [24].

The best enhancement in T_m and T_d has been achieved for the CMCPpy-2 sample, suggesting it for potential applications. Furthermore, the shift in the position of degradation temperature (T_d) for the blended samples to high temperature demonstrated that the addition of PPy enhanced the thermal stability of the CMC matrix, which reflects the formation of strong intermolecular interaction between the PPy as a filler and the CMC structure, confirming the FT-IR results [25].

3.3 Dielectric spectral analysis

3.3.1 Dielectric constant and dielectric loss

Dielectric spectroscopy is useful for studying dielectric materials' crystal structure, grain, grain boundary, charge storage capacity, and transport properties [26]. A real part ε' represents complex dielectric

Table 1 the prepared samples FT-IR absorption bands positions and their assignments

	Vibrational frequency (cm ⁻¹)					Band assignment
	Pure CMC	CMCPpy-1	CMCPpy-2	CMCPpy-3	CMCPpy-4	
	3567	3567	–	–	3566	N–H stretching
	3200	3196	3198	3422	3421	O–H stretching
	2923	2923	2923	2924	2923	C–H stretching
	1720	1733	1733	1733	1733	CO absorption in –COOH
	1589	1587	1588	1589	1589	C=O stretching (CMC)
	–	–	1456	1456	1456	C–N or C=N stretching (PPy)
	1415	1416	1416	1417	1417	C–H scissoring
	1323	1323	1322	1321	1321	O–H bending
	1102	1102	1103	1103	1104	C–O stretching (CMC)
	1055	1056	1056	1056	1056	C–O stretching in CMC.
	1016	1003	1006	1005	1006	CH–O–CH ₂ Stretching
	899	899	–	899	897	C–O Rocking

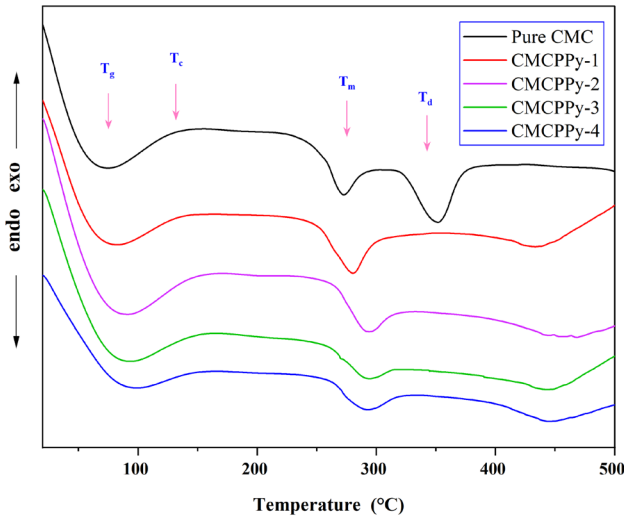


Fig. 2 DSC thermograms of pure CMC and CMC/PPy blends up to 500 °C

Table 2 T_g , T_c , T_m , T_d for pure CMC and CMCPPy-x (x = 1, 2, 3 and 4) blends

Sample	T_g (°C)	T_c (°C)	T_m (°C)	T_d (°C)
Pure CMC	73	139	272	355
CMCPPy-1	80	142	280	435
CMCPPy-2	87	152	295	467
CMCPPy-3	90	157	294	445
CMCPPy-4	93	156	293	446

permittivity (dielectric constant), and ϵ'' (dielectric loss) according to the following relation:

$$\epsilon = \epsilon' + i\epsilon'' \tag{1}$$

The experimental values of ϵ' and ϵ'' can be calculated using:

$$\epsilon' = \frac{LC}{A\epsilon_0} \tag{2}$$

$$\epsilon'' = \frac{\sigma_{ac}}{\omega\epsilon_0} \tag{3}$$

where L is the thickness of a film under investigation, A is its cross-sectional area, C is the sample capacitance measured in parallel mode, ϵ_0 ($= 8.85 \times 10^{-12} \text{F/m}$) is the free space permittivity and ω is the angular frequency.

Figure 3 shows the frequency dependence of (ϵ') of pure CMC and the CMC samples filled with 4, 8, 10, and 12 wt% of PPy at 298 K for all blended samples. As seen in this figure, the CMC curve exhibits that its

dielectric property is similar to other polyelectrolytes and has a unipolar rather than dipolar electric structure [27]. The main reason for originating of electric dipoles inside the host matrix is the imbalance in the distribution of electrons that belongs to the polar functional groups in CMC and PPy monomers, such as COOH, C=O, -OH, and N-H. At low frequencies, ϵ' has gained greater values. As these dipoles align themselves with the electric field, their polarization increases. They have a proclivity for absorbing moisture from the environment, which increases the dielectric constant and decreases resistance [28].

The decrease in ϵ' with increasing frequency for all samples at 298 K could be either due to a reduction in the number of dipoles contributing to polarization or due to the inability of dipole structures to align themselves with the rapid change in the direction of the applied electric field. This minimizes the possibility of electrons reaching the grain boundary and hence polarization, reducing the dielectric constant [29]. Further, Koop’s phenomenological theory [30] revealed that at low frequencies, the high value of dielectric constant originated from the high resistivity of grain boundaries. Whereas, at high frequency, the dielectric constant derived from the grains has a small dielectric constant value due to low resistivity [29].

Figure 4 depicts the ϵ'' curves versus frequency for the above-mentioned samples. The electrically conductive nature of PPy contributes to the significant increase in (ϵ'') when adding it to the CMC matrix.

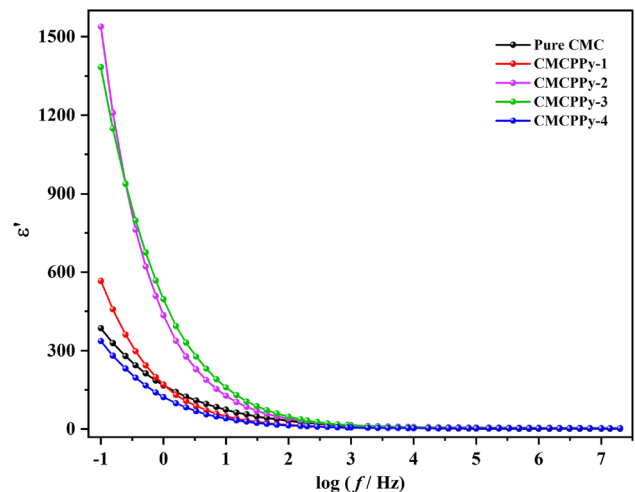


Fig. 3 Frequency dependency of ϵ' for all the CMC/PPy blend samples at room temperature

According to Koop's phenomenological theory, dielectric constant dispersion is connected with Maxwell–Wagner type polarization. Also, according to this hypothesis for inhomogeneous structure, the production of highly conducting grains (PPy) with thin layers of poorly conducting grain boundaries (CMC) occurs during the synthesis of blends, acting as heterogeneous dielectric materials. The ϵ' and ϵ'' values of the present samples at 100 Hz and 10 kHz are summarized in Table 3. At low frequencies, grain boundaries are more effective, so they are the main reason for attaining (ϵ') and (ϵ'') high values. But when the frequency increases, highly conducting grains come into action, causing the dielectric constants to decrease [26]. In other words, ϵ'' decreases as frequency and PPy concentration increase at a constant temperature. The contribution for dc conduction at low and intermediate frequencies is represented by the imaginary component of the dielectric constant. When concentration increases, conductivity increases, resulting in a high value of ϵ'' . This is consistent with the relationship number (3) in the frequency range investigated because ac conductivity might be misled with dc conductivity at low frequencies [31].

The high values of (ϵ'), representing the amount of energy stored, are attributed to either an enhanced conductivity, interfacial polarization, electrode polarization, or all of these factors. This is particularly true at low frequencies. Electrode polarization (EP) is caused by space charges at the electrode-sample interfaces and has extremely high (ϵ') and (ϵ'')

values [28]. All samples were analyzed under identical circumstances and had comparable contents. Consequently, if EP had the highest influence in one sample, it would also be the most influential in all other samples. Considering this, conductivity and interfacial polarization are given a large value for (ϵ'). The 8 wt% PPy (CMCPPy-2) sample acquired the highest electrical improvement and is therefore recommended for application in the development of energy storage devices.

The decrease in (ϵ') and (ϵ''), as observed in Table 3 with increasing PPy concentration, can be ascribed to an improvement in the weakly bonded molecules between the two polymers in the current blends, resulting in a stronger coupling across the grain boundary. This is consistent with the fact that weaker bonds respond more readily to alternating electric fields than stronger bonds [32]. Some studies [28, 33, 34] have found a comparable increase in dielectric constant with increasing filler concentration in the polymer matrix. This increase is due to the presence of conducting PPy, which causes the formation of micro capacitors inside the CMC matrix.

3.4 Electric modulus analysis

An electric relaxation occurs as a result of the mutual movement of dipoles and charges. The dielectric relaxation behavior results from a combination of two polarization mechanisms (interfacial and space charge polarizations). They depend on the physical charges' movement responsible for the dipoles and the time required for the displacement [35].

The formalism electrical modulus is applied to investigate the electrical relaxation mechanism within ion-conducting materials and exploit its advantage of suppressing the electrode polarization effect.

The following relation can be used to express the electrical modulus.

$$M^* = M' + iM'' \quad (4)$$

where the real (M') and imaginary (M'') parts of the electrical modulus are given by:

$$M'' = \frac{\epsilon''}{(\epsilon'^2 + \epsilon''^2)} \quad (5)$$

$$M' = \frac{\epsilon'}{(\epsilon'^2 + \epsilon''^2)} \quad (6)$$

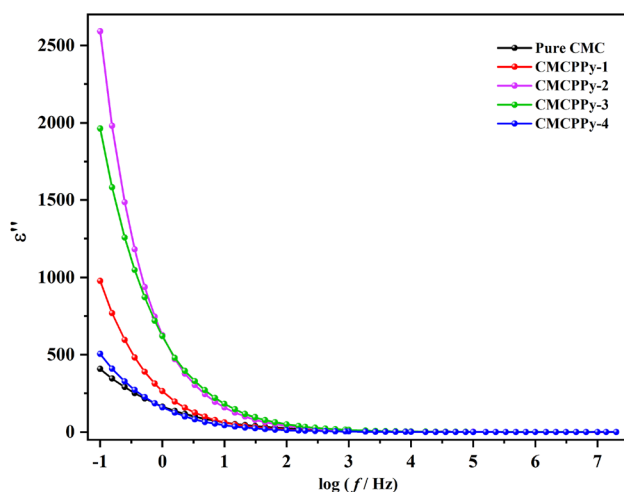


Fig. 4 The dependency on Frequency for (ϵ'') for all the CMC/PPy blend samples at temperature

Table 3 The values of ϵ' , ϵ'' and σ_{ac} at 100 Hz and 10 kHz

Sample	ϵ'		ϵ''		σ_{ac} (S/cm)	
	100 Hz	10 kHz	100 Hz	10 kHz	100 Hz	10 kHz
Pure CMC	31.567	3.37845	24.3614	3.4938	1.355×10^{-9}	1.94373×10^{-8}
CMCPPy-1	15.62	2.94856	16.0432	1.1433	8.925×10^{-10}	6.36045×10^{-9}
CMCPPy-2	39.1541	7.50124	40.0132	2.9266	2.226×10^{-9}	1.62814×10^{-8}
CMCPPy-3	46.9048	5.4175	49.6113	3.12075	2.76×10^{-9}	1.73615×10^{-8}
CMCPPy-4	13.5273	3.05233	12.2577	0.93071	6.819×10^{-10}	5.1778×10^{-9}

Figure 5 represents the frequency dependence of M' at room temperature, where the spectra are distinguished by a sigmoid shape. At low frequencies, M' approaches 0 in all samples, indicating that electrode polarization has a minor effect. M' , on the other hand, reaches its maximum value at higher frequencies. The conductivity relaxation process may be responsible for the dispersion between these frequencies. With increasing frequency, it exhibits a step-like transition [31]. The charge carriers' short-range mobility could explain the continued dispersion with increasing frequency.

Figure 6 represents the frequency dependency of M'' at room temperature which is characterized by the existence of a relaxation peak. As the concentration is increased, the peak shifts to lower frequencies and is associated with an increase in the peak broadness. The peak asymmetrical broadness indicates a variation in relaxation time with distinct time constants, signifying that the material has a non-Debye relaxation type. The two apparent relaxation zones can be interpreted as follow; The left side of the

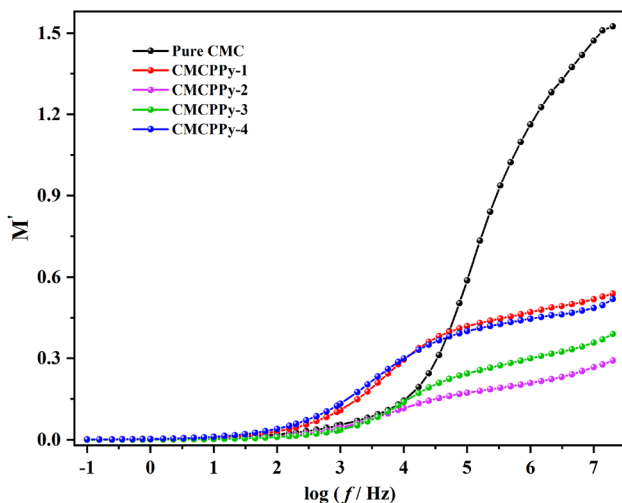


Fig. 5 The dependency on frequency of (M') for the CMC-based samples at room temperature

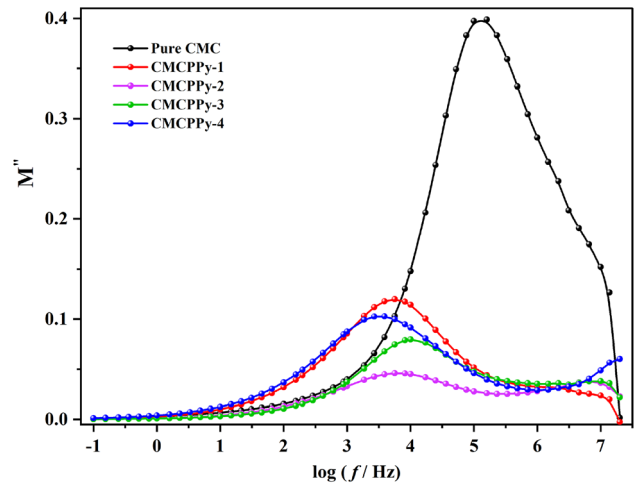


Fig. 6 The dependency on frequency of (M'') for the CMC-based samples at room temperature

asymmetric peak represents charge carrier conduction over a long distance, whereas the right side represents charges confined to a potential well [35].

Both the step-like transition and dispersion occurred in the loss peak are located at a frequency [known as relaxation frequency (f_{max})]. In other words, the transition occurred from long-range charge carrier motion [low-frequency side left to f_{max}] to short-range charge carrier motion [high-frequency side right to f_{max}]. The decrease in M'' with increased PPy especially at CMCPPy-2 sample loading gives a clear indication of the CMC/PPy interaction in the produced blend. This decline behavior is consistent with the Maxwell–Wagner–Sillars (MWS) relaxation model. Interfacial polarization has resulted from the difference in the conductive and dielectric natures of PPy and CMC, where an increase in PPy content produces additional interfacial areas and promotes free charge carrier accumulation in these regions. This accumulation resulted in a decrease in relaxation time (τ_m) as observed from the shift in relaxation peak towards lower frequencies, supporting the

previous results [28]. The calculated values of τ_m are listed in Table 4.

3.5 Dielectric loss tangent

In polymeric materials, dielectric loss is related to the phonon's perturbation caused by the applied electric field. Figure 7 depicts the dependence of loss tangent ($\tan \delta$) on frequency at 298 K for the investigated CMC/PPy blends, as calculated by the following equation [28].

$$\tan \delta = \frac{\epsilon''}{\epsilon'} \quad (7)$$

Dielectric relaxation mechanisms within the current system may be better understood by careful examination of this dependency. The occurrence of a strong relaxation peak in the CMC spectrum is attributed to the dipolar relaxation process of the polymeric parts. For the CMC-based blends, this peak is changed to a shoulder peak due to the incorporation of PPy into the CMC host matrix. This peak has asymmetrical behavior, affirming the semicrystalline nature of the CMC/PPy blends [13]. The addition of polypyrrole shifted the peak in carboxymethyl cellulose toward lower frequency values, indicating that the dynamic became slower.

β -relaxation may be responsible for the observed peak in relaxation in the present investigation; this may be related to the orientation of the polar groups (N-H, OH, and/or C=O) in the polymer blend structure. This is called a relaxation of dipolar group. In the amorphous state, the weak molecular packing and the low density consequently cause the conductivity to increase. The chains in the amorphous phase are irregular, entangled, more flexible, and can orient themselves significantly more easily and quickly. In the side chain of (CMC/PPy), the dipoles of N-H and C=O groups will orient themselves with certain frequencies governed by the elastic restoring force. The force locks the dipoles into place, preventing them

Table 4 The values of relaxation time related to loss tangent

Sample	Tan δ	f_{\max} (Hz)	τ_m (sec)
Pure CMC	1.065	17180.6	9.26×10^{-6}
CMCPPy-1	0.8055	879.213	1.81×10^{-4}
CMCPPy-2	0.898	288.397	5.52×10^{-4}
CMCPPy-3	1.109	1000	1.6×10^{-4}
CMCPPy-4	0.81	289.397	5.5×10^{-4}

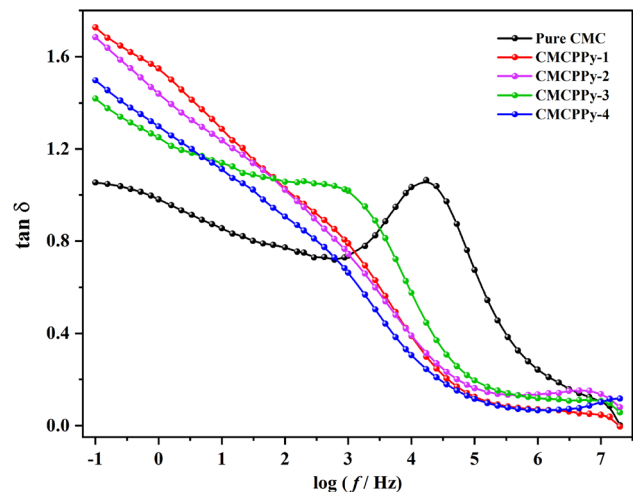


Fig. 7 The dependency on frequency of loss tangent for the CMC-based samples at room temperature

from shifting or spinning in response to the frictional forces of their neighbors [36].

The induced charge carriers (ions/electrons) and the polymeric fragments migrate, leading to dipolar relaxation (i.e., γ -relaxation) and the appearance of a second peak in the high-frequency area for the CMCPPy-2 sample [37].

The decrease in $\tan \delta$ with the frequency is due to the domination of capacitive elements over the Ohmic components inside the present samples [38]. Notably, the CMCPPy-2 sample had the greatest overall performance. It indicates the successful compatibility of CMC with PPy, supporting the XRD and FT-IR results, where this sample has the highest ratio of amorphous areas, making it a good candidate for use in producing polymer-based batteries.

3.6 AC electrical conductivity studies

3.6.1 Electrical conduction mechanism

Figure 8 displays, at 298 K, the frequency dependence of the AC conductivity (σ_{ac}) of the aforementioned blend films. An increase in PPy led to a predominance of amorphous regions, which facilitated the propagation of induced charge carriers and gave rise to the observed increase in σ_{ac} . The CMCPPy-2 sample has significantly enhanced conductivity compared to other concentrations. With increased frequency, electrical conductivity improves because more charge carriers have time to relax by bouncing back and forth between localized locations.

This advancement may be attributed to the shift in hopping behavior from long-range to short-range distances.

The σ_{ac} curves may be understood in part through the jump relaxation model. Using the model, we can estimate how likely it will return to its original starting location, given the proportion of hops that work. (i.e., it returns to its original site). The variation in this ratio between successful and unsuccessful hops accounts for the dispersion in the σ_{ac} values measured for the CMC-based blend samples. Therefore, using Jonscher’s universal power-law, one is able to understand the electrical conductivity of samples, and this interpretation is expressed as follows [18, 38];

$$\sigma = \sigma_{dc} + A\omega^S \tag{8}$$

where A is a factor that depends on temperature. S is a frequency exponent, which affects by the translational movement of the induced charge carriers during the electrical conduction process inside the CMC/PPy blends.

It is clear that the pure CMC curve exhibits frequency dependence with the value of AC conductivity ranged from 2.26×10^{-11} S/cm at 0.1 Hz to 4.24×10^{-7} S/cm at 13.8 MHz. After being filled with PPy, the CMC-based samples show a significant rise in AC conductivity values of about 3.18×10^{-6} S/cm for CMCPy-2 sample, clearly owing to the PPy spread in CMC matrices with

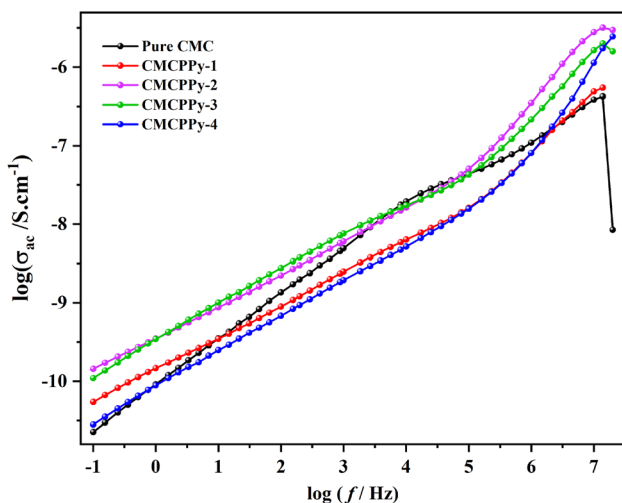


Fig. 8 The frequency dependence of the AC conductivity (σ_{ac}) of the aforementioned blend films at 298 K

content above or close to the percolation threshold. Table 3 shows the σ_{ac} values at 100 Hz and 10 kHz to observe the enhancement in its values for the various concentrations of PPy. Similar results have been reported in the literature [8, 11, 39]. These findings indicate that the investigated CMC-filled films had desired qualities, making them a great starting point for developing cutting-edge devices that store energy.

3.7 M''/M' scale

Figure 9 depicts the Cole-Cole (M' vs. M'') curves for the present samples. It is obvious that the modulus spectra change in size and form with increasing PPy concentration, which means that the capacitance values are concentration dependent. The conductivity relaxation is indicated by the semicircular arc.

There are three distinct sectors in the Cole-Cole plot, each corresponding to a different frequency range. The three zones may be understood as a result of three distinct processes: the grain boundary effect, the involvement of grains, and the bulk conduction relaxation process [2]. The CMC spectrum shows a single semi-circular peak, indicating the existence of one kind of relaxation phenomenon with a relaxation time (τ_m). This single arc is also ascribed to the grain boundary effect and surface polarization. The relaxation peak’s asymmetrical characteristic proves the non-Debye dielectric relaxation response [35]. When PPy was added at different concentrations of PPy, two semi-circular peaks arose, indicating two types

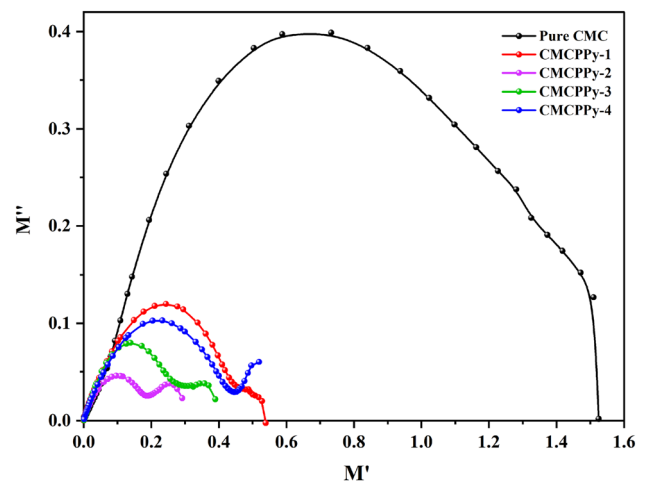


Fig. 9 The Cole-Cole (M' vs. M'') curves for the present samples

Table 5 The values of resistance (R_{gb}), capacitance (C_{gb}), M''_{max} , f_{max} and the relaxation time (τ_{gb}) corresponding to electrical parameters of the grain boundary

Sample	M''_{max}	f_{max} (Hz)	τ_m (sec)	C (F)	R (Ω)
Pure CMC	0.398073	1,29,839	1.1798×10^{-6}	1.114×10^{-11}	1,06,290
CMCPPy-1	0.11985	5635.52	2.82×10^{-5}	3.69×10^{-11}	7,65,148
CMCPPy-2	0.045835	6903.51	2.73×10^{-5}	9.64×10^{-11}	2,82,945
CMCPPy-3	0.07984	10,000	1.59×10^{-5}	5.6×10^{-11}	2,84,205
CMCPPy-4	0.102695	3283.475	4.186×10^{-5}	4.338×10^{-11}	9,64,980

of relaxation phenomena. In other words, the dielectric relaxation behavior has resulted from a combination of two polarization mechanisms.

One of the mechanisms stems from the polymer's dielectric properties, which is frequently linked with dipoles reorientation, particularly the OH polar groups, whereas the second mechanism is caused by the presence of carbon particles. Therefore, the plot displays a tendency of two deformed semicircles, showing the presence of both grain and grain boundary contributions in the blended film.

At the CMC/PPy interface, Maxwell–Wagner–Silars (MWS) polarization mechanism leads to an accumulation of electric charges stemmed from the additives, fillers, and even impurities, making the polymeric blends heterogeneous. So interfacial polarization is nearly always present in their systems [40].

The peak in the low-frequency range suggests that ions travel long distances, whereas the high-frequency peak suggests that ions shift short distances due to confining in their potential well [41]. At low frequencies, the small semicircular arcs represent the contribution of weak grain boundary effects rather than the dominant grain effects. The bulk or grain response is represented by the huge semicircular arches at high frequency [41]. These spectra are composed of a semicircular arc that may be modeled by combining a resistor and a constant phase element (CPE1) in parallel. The low-frequency spike region found in PPy-containing materials may be modeled using a second constant phase element (CPE2). The following equation governs the relaxation peak frequencies:

$$f_{max} \approx \frac{1}{2\pi RC} \quad (9)$$

In this equation, the peak frequency is related to the capacitance of the geometrical capacitor in a way that is inversely proportional to that value. The values of the resistance (R_{gb}), capacitance (C_{gb}), maximum frequency, M''_{max} and relaxation time (τ_{gb}) corresponding to electrical parameters of the grain boundary are listed in Table 5. The change observed in their values demonstrates the constructive effect of PPy. The CMCPPy-2 sample acquired the maximum capacitance, making it highly recommended for use in the construction of electrical double-layer capacitors. This is in contrast to the observed shift in the f_{max} towards the lower frequency zone. This change also demonstrates the minor role played by the grain boundary in the CMC host matrix's electrical conduction process. Due to the dipoles' rotation, the CMCPPy-2 sample's existing film is more capacitive than resistive, giving it a significant performance edge over competing blends.

4 Conclusion

Different hybrid polymer blends based on sodium carboxymethyl cellulose and polypyrrole (CMC-PPy) were created using a solution casting approach with varying PPy weight percentages (4, 8, 10, and 12 wt%). DSC curves concluded that PPy loaded CMC matrix with minor differences in concentrations of PPy displayed an overall enhancement and reinforced the thermal stability of CMC/PPy blends. Evidence of distinct displacement dynamics for the induced ions may be seen in the transition from long-range to short-range ion motion. The relaxation dynamics and

conductivity relaxation within the current samples were elucidated using the scaling approach. AC conductivity of the pure CMC sample ranged from 2.26×10^{-11} S/cm at 0.1 Hz to 4.24×10^{-7} S/cm at 13.8 MHz. After being filled with PPy, the CMC-based samples exhibited a significant rise in AC conductivity values of about 3.18×10^{-6} S/cm for the CMCPy-2 sample. Moreover, the best enhancement in thermal stability and dielectric properties has been achieved for the CMCPy-2 sample, suggesting it for potential applications. Because of their different nature, the CMC and PPy gave rise to novel interfacial areas. This distinction also played an important part in forming micro-capacitors inside the present host matrix, which improved the product's dielectric characteristics.

Author contributions

AMS: Data curation, methodology, validation, formal analysis, investigation, conceptualization, writing—original draft. ARM: Data curation, methodology, formal analysis, conceptualization, supervision. AYY: Resources, data curation, methodology, validation, formal analysis, investigation, conceptualization, supervision, software, visualization, writing—original draft, writing—review and editing.

Funding

Open access funding provided by The Science, Technology & Innovation Funding Authority (STDF) in cooperation with The Egyptian Knowledge Bank (EKB).

Data availability

All data generated or analyzed during this study are included in this article and are available with the authors.

Declarations

Conflict of interest The authors declare that we have no known competing financial interests or personal relationships that could have appeared to influence the work reported in this paper.

Open Access This article is licensed under a Creative Commons Attribution 4.0 International License, which permits use, sharing, adaptation, distribution and reproduction in any medium or format, as long as you give appropriate credit to the original author(s) and the source, provide a link to the Creative Commons licence, and indicate if changes were made. The images or other third party material in this article are included in the article's Creative Commons licence, unless indicated otherwise in a credit line to the material. If material is not included in the article's Creative Commons licence and your intended use is not permitted by statutory regulation or exceeds the permitted use, you will need to obtain permission directly from the copyright holder. To view a copy of this licence, visit <http://creativecommons.org/licenses/by/4.0/>.

References

1. M. Sai, D. Sethy, S. Francis, M.S.Y. Kumar, F.V. Varghese, K. Balasubramaniam, Optical properties of multilayer graphene nanoplatelet (mGNP)/poly(methyl methacrylate) (PMMA) composite flexible thin films prepared by solvent casting. *J. Mater. Sci. Mater. Electron.* **32**, 26750–26757 (2021)
2. A.M. Salem, A.R. Mohamed, A.M. Abdelghany, A.Y. Yassin, Effect of polypyrrole on structural, optical and thermal properties of CMC-based blends for optoelectronic applications. *Opt. Mater.* **134**, 113128 (2022)
3. A. Patra, M. Bendikov, S. Chand, Poly (3, 4-ethylenedioxy-selenophene) and its derivatives: novel organic electronic materials. *Acc. Chem. Res.* **47**(5), 1465–1474 (2014)
4. G. Burwell, N. Burrige, E. Bond, W. Li, P. Meredith, A. Armin, Parameterization of metallic grids on transparent conductive electrodes for the scaling of Organic Solar cells. *Adv. Electron. Mater.* **7**(6), 2100192 (2021)
5. A.Y. Yassin, A.M. Abdelghany, Synthesis and thermal stability, electrical conductivity and dielectric spectroscopic studies of poly (ethylene-co-vinyl alcohol)/graphene oxide nanocomposite. *Phys. B Condens. Matter* **608**, 412730 (2021)
6. A.Y. Yassin, A.R. Mohamed, E.M. Abdelrazek, M.A. Morsi, A.M. Abdelghany, Structural investigation and enhancement of optical, electrical and thermal properties of poly(vinyl chloride-co-vinyl acetate-co-2-hydroxypropyl acrylate)/graphene oxide nanocomposites. *J. Mater. Res. Technol.* **8**, 1111–1120 (2019)
7. E.M. Abdallah, G.M. Asnag, M.A. Morsi, M. Aljohani, A.N. Albalwa, A.Y. Yassin, Elucidation of the effect of hybrid

- copper/selenium nanofiller on the optical, thermal, electrical, mechanical properties and antibacterial activity of polyvinyl alcohol/carboxymethyl cellulose blend. *Polym. Eng. Sci.* **63**, 1974–1988 (2023). <https://doi.org/10.1002/pen.26339>
8. A.Y. Yassin, Synthesized polymeric nanocomposites with enhanced optical and electrical properties based on gold nanoparticles for optoelectronic applications. *J. Mater. Sci. Mater. Electron.* **34**, 46 (2023). <https://doi.org/10.1007/s10854-022-09402-3>
 9. H. Huang, P. He, N. Hu, Y. Zeng, Electrochemical and electrocatalytic properties of myoglobin and hemoglobin incorporated in carboxymethyl cellulose films. *Bioelectrochemistry* **61**, 29–38 (2003)
 10. M.P. Adinugraha, D.W. Marseno, Synthesis and characterization of sodium carboxymethylcellulose from cavendish banana pseudo stem (*Musa cavendishii* LAMBERT). *Carbohydr. Polym.* **62**, 164–169 (2005)
 11. A.Y. Yassin, A.M. Abdelghany, R.S. Salama, A.E. Tarabiah, Structural, optical and antibacterial activity studies on CMC/PVA Blend filled with three different types of Green synthesized ZnO nanoparticles. *J. Inorg. Organomet. Polym. Mater.* (2023). <https://doi.org/10.1007/s10904-023-02622-y>
 12. Y. Bu, H.X. Xu, X. Li, W.J. Xu, Y.X. Yin, H.L. Dai, X.B. Wang, Z.J. Huang, P.H. Xu, A conductive sodium alginate and carboxymethyl chitosan hydrogel doped with polypyrrole for peripheral nerve regeneration. *RSC Adv.* **8**(20), 10806–10817 (2018). <https://doi.org/10.1039/c8ra01059e>
 13. N. Yusoff, Graphene–polymer modified electrochemical sensors. *Graphene-Based Electroche Sens Biomol* (2019). <http://doi.org/10.1016/B978-0-12-815394-9.00007-8>
 14. S. Dey, A.K. Kar, Effect of PPy concentration on the photoluminescence of PPy–PMMA blends: observation of acceptor concentration-dependent FRET. *J. Mater. Sci. Mater. Electron.* **33**, 9018–9030 (2022). <https://doi.org/10.1007/s10854-021-07092-x>
 15. S. Uzunçar, N. Özdoğan, M. Ak, Amperometric detection of glucose and H₂O₂ using peroxide selective electrode based on carboxymethylcellulose/polypyrrole and prussian blue nanocomposite. *Mater. Today Commun.* **26**, 101839 (2021)
 16. A.A. Al-Muntaser, R.A. Pashameah, A. Saeed, R. Alwafi, E. Alzahrani, S.A. AlSubhi, A.Y. Yassin, Boosting the optical, structural, electrical, and dielectric properties of polystyrene using a hybrid GNP/Cu nanofiller: novel nanocomposites for energy storage applications. *J. Mater. Sci.: Mater. Electron.* **34**, 678 (2023). <https://doi.org/10.1007/s10854-023-10104-7>
 17. Y. Wang, L. Zhu, L. An, Electricity generation and storage in microbial fuel cells with porous polypyrrole-base composite modified carbon brush anodes. *Renew. Energy* **162**, 2220–2226 (2020). <https://doi.org/10.1016/j.renene.2020.10.032>
 18. Y. Wang, X. Pan, Y. Chen, Q. Wen, C. Lin, J. Zheng, W. Li, H. Xu, L. Qi, A 3D porous nitrogen-doped carbon nanotube sponge anode modified with polypyrrole and carboxymethyl cellulose for high-performance microbial fuel cells. *J. Appl. Electrochem.* **50**(12), 1281–1290 (2020). <https://doi.org/10.1007/s10800-020-01488-z>
 19. N.F. Mazuki, A.P.P. Abdul Majeed, Y. Nagao, A.S. Samsudin, Studies on ionics conduction properties of modification CMC-PVA based polymer blend electrolytes via impedance approach. *Polym. Test.* **81**, 106234 (2020). <https://doi.org/10.1016/j.polymertesting.2019.106234>
 20. N.S. El-Sayed, M.A. Moussa, S. Kamel, G. Turkey, Development of electrical conducting nanocomposite based on carboxymethyl cellulose hydrogel/silver nanoparticles@polypyrrole. *Synth. Met.* **250**, 104–114 (2019). <https://doi.org/10.1016/j.synthmet.2019.03.010>
 21. A.S. Samsudin, W.M. Khairul, M.I.N. Isa, Characterization on the potential of carboxy methylcellulose for application as proton conducting biopolymer electrolytes. *J. Non-Cryst Solids* **358**(8), 1104–1112 (2012). <https://doi.org/10.1016/j.noncrysol.2012.02.004>
 22. J.F. Su, Z. Huang, X.Y. Yuan, X.Y. Wang, M. Li, Structure and properties of carboxymethyl cellulose/soy protein isolate blend edible films crosslinked by Maillard reactions. *Carbohydr. Polym.* **79**(1), 145–153 (2010). <https://doi.org/10.1016/j.carbpol.2009.07.035>
 23. N.E. Miri, K. Abdelouahdi, M. Zahouily, A. Fihri, A. Barakat, A. Solhy, M.E. Achaby, Bio-nanocomposite films based on cellulose nanocrystals filled polyvinyl alcohol/chitosan polymer blend. *J. Appl. Polym. Sci.* **132**, 42004 (2015). <https://doi.org/10.1002/app.42004>
 24. A. Batool, F. Kanwal, M. Imran, T. Jamil, S.A. Siddiqi, Synthesis of polypyrrole/zinc oxide composites and study of their structural, thermal and electrical properties. *Synth. Met.* **161**, 23–24 (2012). <https://doi.org/10.1016/j.synthmet.2011.10.016>
 25. G.M. Asnag, A.H. Oraby, A.M. Abdelghany, Green synthesis of gold nanoparticles and its effect on the optical, thermal and electrical properties of carboxymethyl cellulose. *Compos. Part. B Eng.* **172**, 436–446 (2019). <https://doi.org/10.1016/j.compositesb.2019.05.044>
 26. R.S. Yadav, I. Kuřitka, J. Vilcakova, J. Havlica, L. Kalina, P. Urbánek, M. Machovsky, M. Masař, M. Holec, Influence of La³⁺ on structural, magnetic, dielectric, electrical and modulus spectroscopic characteristics of single phase CoFe_{2-x}La_xO₄ nanoparticles. *J. Mater. Sci. Mater. Electron.* **28**(12), 9139–9154 (2017). <https://doi.org/10.1007/s10854-017-6648-5>
 27. S. El-Sayed, K.H. Mahmoud, A.A. Fatah, A. Hassen, TGA and dielectric properties of carboxymethyl cellulose/polyvinyl

- alcohol blends. *Phys. B Condens. Matter* **406**(21), 4068–4076 (2011). <https://doi.org/10.1016/j.physb.2011.07.050>
28. A.Y. Yassin, A.R. Mohamed, A.M. Abdelghany, E.M. Abdelrazek, Enhancement of dielectric properties and AC electrical conductivity of nanocomposite using poly (vinyl chloride-co-vinyl acetate-co-2-hydroxypropyl acrylate) filled with graphene oxide. *J. Mater. Sci. Mater. Electron.* **29**(18), 15931–15945 (2018). <https://doi.org/10.1007/s10854-018-9679-7>
29. P. Chand, S. Vaish, P. Kumar, Structural, optical and dielectric properties of transition metal (MFe_2O_4 ; $M=Co, Ni$ and Zn) nanoferrites. *Phys. B Condens. Matter* **524**, 53–63 (2017). <https://doi.org/10.1016/j.physb.2017.08.060>
30. C.G. Koops, On the dispersion of resistivity and dielectric constant of some semiconductors at audio frequencies. *Phys. Rev.* **83**(1), 121–124 (1951)
31. S.F. Chérif, A. Chérif, W. Dridi, M.F. Zid, Ac conductivity, electric modulus analysis, dielectric behavior and bond valence sum analysis of $Na_3Nb_4As_3O_{19}$ compound. *Arab. J. Chem.* **13**(6), 5627–5638 (2020). <https://doi.org/10.1016/j.arabj.2020.04.003>
32. A. Abdel-Galil, H.E. Ali, A. Atta, M.R. Balboul, Influence of nanostructured TiO_2 additives on some physical characteristics of carboxymethyl cellulose (CMC). *J. Radiat. Res. Appl. Sci.* **7**(1), 36–43 (2014). <https://doi.org/10.1016/j.jrras.2013.11.004>
33. K. Sundaramahalingam, D. Vanitha, N. Nallamuthu, A. Manikandan, M. Muthuvinayagam, Electrical properties of lithium bromide poly ethylene oxide / poly vinyl pyrrolidone polymer blend electrolyte. *Phys. B Condens. Matter* **553**, 120–126 (2019)
34. H.N.M.E. Mahmud, A. Kassim, Z. Zainal, W.M.M. Yunus, Electrochemical formation of polypyrrole-carboxymethylcellulose conducting polymer composite films. *J. Mater. Sci. Technol.* **21**(5), 661–665 (2005)
35. M. Halder, A.K. Meikap, Dielectric relaxation and current conduction mechanism of tb and mn codoped bismuth ferrite grafted poly (vinyl alcohol) nanocomposite film. *Rev. Adv. Mater. Sci.* **59**(1), 425–433 (2020). <https://doi.org/10.1515/rams-2020-0040>
36. E.M. Abdelrazek, I.S. Elashmawi, A. El-Khodary, A. Yassin, Structural, optical, thermal and electrical studies on PVA/PVP blends filled with lithium bromide. *Curr. Appl. Phys.* **10**(2), 607–613 (2010)
37. N. Alberola, J.Y. Cavaille, Perez Mechanical spectrometry of alpha relaxations of high-density polyethylene. *J. Polym. Sci. B Polym. Phys.* **28**, 569–586 (1990)
38. A. Arya, A.L. Sharma, Effect of salt concentration on dielectric properties of Li-ion conducting blend polymer electrolytes. *J. Mater. Sci. Mater. Electron.* **29**, 17903–17920 (2018)
39. A.A. Al-Muntaser, R.A. Pashameah, K. Sharma, E. Alzaharani, S.T. Hameed, M.A. Morsi, Boosting of structural, optical, and dielectric properties of PVA/CMC polymer blend using $SrTiO_3$ perovskite nanoparticles for advanced optoelectronic applications. *Opt. Mater.* **132**, 112799 (2022)
40. S. Boukheir, Z. Samir, R. Belhimria, L. Kreit, M.E. Achour, N. Éber, L.C. Costa, A. Oueriagli, A. Outzourhit, Electric Modulus Spectroscopic Studies of the Dielectric Properties of Carbon Nanotubes/Epoxy Polymer Composite materials. *J. Macromol. Sci. Part. B Phys.* **57**(3), 210–221 (2018). <https://doi.org/10.1080/00222348.2018.1439243>
41. M. Coşkun, A.O. Polat, F.M. Coşkun, Z. Durmuş, C.M. Caglar, A. Türüt, The electrical modulus and other dielectric properties by the impedance spectroscopy of $LaCrO_3$ and $LaCr_{0.90}Ir_{0.10}O_3$ perovskites. *RSC Adv.* **8**(9), 4634–4648 (2018). <https://doi.org/10.1039/c7ra13261a>

Publisher's Note Springer Nature remains neutral with regard to jurisdictional claims in published maps and institutional affiliations.